

## Article

# Dynamic Analysis for a Reciprocating Compressor System with Clearance Fault

Shungen Xiao <sup>1,\*</sup> , Qingfeng Xiao <sup>2</sup>, Mengmeng Song <sup>1</sup> and Zexiong Zhang <sup>1,3</sup>

<sup>1</sup> College of Information, Mechanical and Electrical Engineering, Ningde Normal University, Ningde 352100, China; t1119@ndnu.edu.cn (M.S.); 3191218017@fafu.edu.cn (Z.Z.)

<sup>2</sup> School of Mechatronic Engineering and Automation, Shanghai University, Shanghai 200072, China; xiaoshungen@shu.edu.cn

<sup>3</sup> College of Mechanical and Electrical Engineering, Fujian Agriculture and Forestry University, Fuzhou 350000, China

\* Correspondence: xiaoshungen022@163.com or t0932@ndnu.edu.cn

**Abstract:** In order to explore the failure mechanism of a reciprocating compressor system with clearance fault, we implemented a computational framework whereby a simulation model of the mechanism is established using ADAMS software in this paper, and a typical reciprocating compressor model is introduced to validate the design model. In this work, the joint clearance faults between the crankshaft and linkage, between the linkage and crosshead, and in both locations are taken into account computationally. These faults are one of the major causes of vibration. Through dynamic calculation and analysis of a system with clearance fault, the simulated results show that these clearance faults directly influence the vibration. The larger the gap size, the more severe the vibration and the higher the amplitude of the vibration. Furthermore, the clearance number also affects the vibration greatly.

check for  
updates

**Citation:** Xiao, S.; Xiao, Q.; Song, M.; Zhang, Z. Dynamic Analysis for a Reciprocating Compressor System with Clearance Fault. *Appl. Sci.* **2021**, *11*, 11295. <https://doi.org/10.3390/app112311295>

**Keywords:** computational analysis; reciprocating compressor; translational mechanism; clearance fault; vibration

Academic Editor:

Alessandro Gasparetto

Received: 10 October 2021

Accepted: 15 November 2021

Published: 29 November 2021

**Publisher's Note:** MDPI stays neutral with regard to jurisdictional claims in published maps and institutional affiliations.



**Copyright:** © 2021 by the authors. Licensee MDPI, Basel, Switzerland. This article is an open access article distributed under the terms and conditions of the Creative Commons Attribution (CC BY) license (<https://creativecommons.org/licenses/by/4.0/>).

## 1. Introduction

Reciprocating compressors are widely applied in the petrochemical industry and refrigeration. It often occupies a vital position in the processing system [1]. The health of the compressor is directly related to the production and economic benefits of the enterprise. Due to the severe working environment and the multiple motivating sources, faults frequently occur in the reciprocating compressor, which degrade the production efficiency and even cause serious consequences. However, the complicated structure of the reciprocating compressor makes it challenging to monitor and diagnose the faults. Therefore, the various faults' diagnostic methods and mechanism analysis have been the focus of research on reciprocating compressor systems [2–4].

So far, many researchers have investigated technologies for monitoring and diagnosing the various faults in a reciprocating compressor. Most of them pay attention to the diagnostic methods of broken valves, because valve faults are the most common in a reciprocating compressor. They presented several approaches based on a PV diagram, vibration analysis, or information entropy [5–7]. In addition, some researchers focus on automated classification of the faults in reciprocating compressors [8,9]. However, few of them focus on the failure mechanism of the translational mechanism in the reciprocating compressor system. The translational tool consists of the critical parts of the crankshaft, linkage, crosshead, and piston assembly. Although the number of faults in these parts is less than that for the valves, it always causes more severe consequences, even causing safety accidents. Thus, fault detection and diagnosis for these parts should be concentrated on more.

Compared with the valve, detecting and diagnosing faults in translational machinery is more complex because these parts are always located inside the airtight chamber. At present, the most common and effective fault diagnosis methods for these parts are based on vibration analysis. Chen [10] proposed a three-stage network system to diagnose piston slap faults in reciprocating machines based on vibration signals. Geng [11] developed a piston slap fault model of a reciprocating engine to investigate the vibration response induced by a slap and the relationship between the piston slap impact and the vibration. However, as the author of [11] said, the reciprocating machine vibration properties, such as the impact excitations and time-varying transfer characteristics, make it challenging to obtain a significant signature directly. Therefore, it is necessary to develop a model to compute and simulate the dynamic behaviors of the reciprocating compressor under normal and faulty conditions and investigate the relationship between faults and vibration. Recently, several models of reciprocating compressors have been established for different purposes. Demba [12] proposed a dynamic model of a hermetic reciprocating compressor in on-off cycle operation to analyze the effect of the transient conditions on the mass flow rate of suction, discharge, and electrical power. Yang [13] presented a comprehensive model for a semi-hermetic CO<sub>2</sub> reciprocating compressor to simulate the geometry and kinematics, the compression process, and the frictional power loss. Mahmood [14] developed a thermodynamic model to study the effects of the parameters, including the angular speed, clearance, and pressure ratio, on the performance of the CNG reciprocating compressor. Rodrigo [15] introduced a numerical model of a reciprocating compressor in a startup and shutdown transient to investigate its performance in such transients. These models presented in the above literature are a valuable tool for analyzing or predicting a compressor's thermodynamic behavior, including the flow rate, friction loss, and so on, but they are not suitable for analysis of the vibration or fault detection and diagnosis for translational machinery. The translational mechanism of the reciprocating compressor is a crank-slider mechanism. Some researchers have been trying to apply the achievements of the crank-slider tool to devices. Pont [16] developed a numerical model for a reciprocating compressor mechanism based on the kinematic and dynamic formulation and studied the secondary movements of the piston and crankshaft and their interaction. Almasi [17] built a model of a reciprocating mechanism and took the dynamic force induced by the crosshead into consideration to reduce vibration and optimize the design. Zhao [18] applied the contact force model of the planar joint clearance into the reciprocating compressor dynamic model to study the vibration response induced by an oversized clearance joint fault.

In this paper, to explore the failure mechanism of the translational mechanism based on the analysis of dynamic behavior, a simplified model for the reciprocating compressor is built by ADAMS software. To validate the design model, we also introduce a typical model of the compressor. We also take into account several specific faults in the translational mechanism, including joint clearance faults between the crankshaft and linkage and between the linkage and crosshead. The dynamic response of the instrument under these faults is investigated. We try to analyze the relationship between these oversized clearance joint faults and the vibration of the compressor body.

## 2. Model of the Reciprocating Compressor

In this work, we take a single-stage reciprocating compressor as the research object. The design model is composed of the kinematic mechanism model and the load model for the reciprocating compressor, as shown in Figure 1.

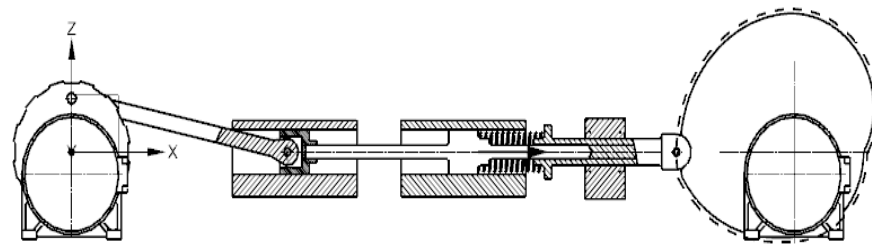


Figure 1. Model structure of the reciprocating compressor.

2.1. Kinematic Mechanism Model

The kinematic mechanism model consists of the crankshaft, linkage, crosshead, piston assembly, and cylinder. The reciprocating compressor, a typical piece of volumetric machinery, utilizes the piston moving in a reciprocating linear motion driven by the crankshaft to compress and deliver the medium gas. Figure 2 shows the schematic diagram of the compressor. As shown in Figure 2, the crankshaft rotates with a constant speed, driven by a motor. Although the crankshaft rotates the entire circumference and is driven by the connecting rod, the crosshead slider always reciprocates linearly. The crosshead and pistons are connected by a piston rod and fastened by a thread, which is considered part of the same rigid body, and therefore the piston has the same motion with the crosshead.

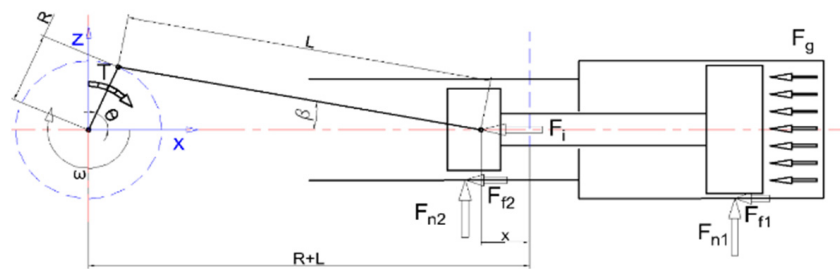


Figure 2. Diagrammatic drawing of the reciprocating compressor.

According to the above analysis, the motion of reciprocating compressor can be described by the displacement of the piston as shown in Equation (1):

$$x = S_0 + R \cdot (1 - \cos \theta) + L \cdot (1 - \sqrt{1 - \lambda^2 \sin^2 \theta}) \tag{1}$$

where  $S_0$  is the clearance volume,  $x$  denotes the displacement of the mechanism,  $R$  represents the crank length,  $\theta$  denotes the angle of rotation for the crankshaft,  $L$  represents the linkage length, and  $\lambda$  denotes the ratio of the crankshaft length to the linkage length.

Unfolded by Taylor, we can obtain the following:

$$\sqrt{1 - \lambda^2 \sin^2 \theta} = 1 - \frac{1}{2} \lambda^2 \sin^2 \theta - \frac{1}{8} \lambda^4 \sin^4 \theta + ([-\lambda^2 \sin^2 \theta]^3) \approx 1 - \frac{1}{2} \lambda^2 \sin^2 \theta = 1 - \frac{1}{4} \lambda^2 (1 - \cos 2\theta) \tag{2}$$

Therefore, Equation (1) can be substituted with Equation (3):

$$x \approx S_0 + R \cdot (1 - \cos \theta) + \frac{\lambda}{4} R \cdot (1 - \cos 2\theta) \tag{3}$$

The velocity and acceleration of the whole motion mechanism can be expressed by using the derivation of the displacement with respect to time as shown in Equation (4):

$$\begin{cases} \dot{x} = R \cdot \omega \cdot (\sin \theta + \frac{\lambda}{2} \cdot \sin 2\theta) \\ \ddot{x} = R \cdot \omega^2 \cdot (\cos \theta + \lambda \cdot \cos 2\theta) \end{cases} \tag{4}$$

### 2.2. Load Model

During the working process of the reciprocating compressor, the loads acting on the mechanism mainly include gas force acting on the piston, the inertia force, and the frictional force, which make up the multiple piston loads. The multiple piston forces equal the vector sum of them and can be calculated with Equation (5):

$$F = F_g + F_i + F_r \tag{5}$$

where  $F_g$  denotes the gas force,  $F_i$  is the inertia force, and  $F_r$  represents the frictional force.

The gas force comes from the cylinder cavity, for which the direction is perpendicular to the face of the piston, and the value is proportional to the cylinder pressure. Note that the working process of a compressor is a complex thermodynamic process, which consists of a suction process, compression process, discharge process, and expansion process. Therefore, the cylinder pressure shows four different variations in one cycle.

In order to simplify the computation, this paper assumes that there is no power loss in the suction and discharge stages, the compression and expansion stages are isentropic, there is no leakage, and the medium gas is an ideal gas. Figure 3 displays the ideal diagrammatic drawing of the cylinder pressure.

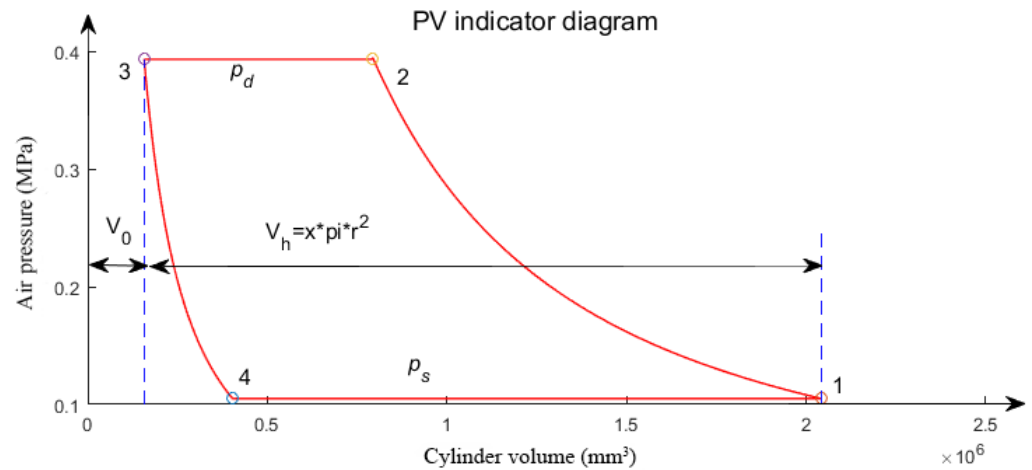


Figure 3. PV indicator diagram of a reciprocating compressor.

After simplification, the relationship between the gas force and the equivalent displacement of the translational mechanism can be obtained with Equation (6):

$$F_g = p \cdot \pi \cdot r^2 = \begin{cases} p_s \cdot \pi \cdot r^2 & \text{Suction phase} \\ p_s \cdot \left(\frac{s+s_0}{x}\right)^m \cdot \pi \cdot r^2 & \text{Compression phase} \\ p_d \cdot \pi \cdot r^2 & \text{Exhaust phase} \\ p_d \cdot \left(\frac{s_0}{x}\right)^m \cdot \pi \cdot r^2 & \text{Expansion phase} \end{cases} \tag{6}$$

where  $p$  represents the cylinder pressure,  $p_s$  and  $p_d$  are the cylinder pressure in the suction stage and the discharge stage, respectively,  $r$  denotes the radius of the piston, and  $s$  represents the piston stroke.

The inertial force of the mechanism consists of the reciprocating inertia force and the rotational inertia force. The reciprocating inertia force is produced by the crosshead and piston assembly that move in a reciprocating motion, for which the value is proportional to the mass and acceleration of the moving parts, and the direction is the opposite of the acceleration of the piston.

The rotational inertia force is mainly caused by the dynamic imbalance of the crankshaft, which can be offset by adding a balance block. Thus, the inertia can be calculated with Equation (7):

$$\begin{cases} F_i = m \cdot \ddot{x} = m \cdot \omega^2 \cdot (\cos \theta + \lambda \cdot \cos 2\theta) \\ m = m_p + 0.5m_{cr} \end{cases} \quad (7)$$

where  $m_p$  represents the mass of the crosshead and piston and  $m_{cr}$  denotes the mass of the linkage.

The frictional force is mainly roused by the relative motion between the piston and the cylinder, crosshead, and sliding way. Compared with the air force, the friction force is so small that it can be ignored.

According to the above analysis, the piston force mainly depends on the gas force, which is difficult to simulate. To achieve simulation of the piston force, this paper designed a load model composed of a plate cam, a translating roller follower, and a cylindroid helical coil compression spring as shown in Figure 1. The cam angle corresponded to the crankshaft angle; in other words, the cam angle in the rise phase, the high-dwell phase, the fall phase, and the low-dwell phase corresponded to the crankshaft angle in the suction process, compression process, discharge process, and expansion process, respectively. The spring was installed between the follower and piston. The minimum load of the spring equaled the piston force during the suction process, and the maximum load of the spring equaled the piston force during the discharge process. The model utilized the deformation force of the spring controlled by the cam mechanism to simulate the piston force. More specifically, the cam and crankshaft ran together with same speed, making the follower perform movement with respect to the piston. The detailed motions were as follows. As the piston moved from the dead end of the cylinder to the crankshaft side, the follower dwelled, making the spring get released from the maximum deformation to the minimum deformation and realizing the falling load. In the suction process, as the piston continued to move to the crankshaft side, the follower rose and moved with the piston at same speed, keeping the spring under the minimum deformation and realizing the minimum constant load. During the compression process, as the piston moved from the crankshaft side to the dead end, the follower dwelled, making the spring get compressed from the minimum deformation to the maximum deformation and realizing a rising load. In the discharge process, as the piston continued to move to the dead end, the follower returned and moved with the piston at the same speed, keeping the spring under the maximum deformation and realizing the maximum constant load.

### 2.3. Spring Design

The minimum service load of the spring is equal to the gas force in the suction process, and the maximum service load of the spring is equal to the gas force in the discharge process, as shown in Equation (8):

$$\begin{cases} P_{\max} = p_d \cdot \pi r^2 \\ P_{\min} = p_s \cdot \pi r^2 \end{cases} \quad (8)$$

The working stroke of the spring is the difference between the maximum deformation and the minimum deformation of the spring, and its value is equal to the displacement of the piston in the compression process:

$$h = x_{pc} - (L - R) \quad (9)$$

where  $x_{pc}$  is the position of the piston at the end of the compression stage.

According to the calculated working load and the stroke [19], we determined the spring's characteristic parameters by referring to *Machinery's Handbook*, including the stiffness, spring diameter, spring wire diameter, the spring coil number, and the initial length.

### 2.4. Design and Calculation of the Cam

According to the above analysis, it is not difficult to know that the displacement of the follower in the rising phase is equal to the displacement of the piston during the suction process, and the displacement of the follower in the return phase is equal to the displacement of the piston in the discharge phase. Therefore, the motion equation of the follower can be obtained with Equation (10):

$$s_c = \begin{cases} X_{pe} - (R \cdot \cos \phi + L \cdot \sqrt{1 - \lambda^2 \cdot \sin^2 \phi}) & \theta_{exp} < \phi < \pi \\ L + R - (R \cdot \cos \phi + L \cdot \sqrt{1 - \lambda^2 \cdot \sin^2 \phi}) & \theta_{comp} < \phi < 2\pi \end{cases} \quad (10)$$

where  $x_{pe}$  is the position of the piston at the end of the expansion stage and  $\phi$  is the cam angle.

According to the allowed pressure angle, this paper determines the cam's basic circle radius and the eccentricity as shown in Equation (11):

$$r_0 \geq \sqrt{\left(\frac{\frac{ds_c}{d\phi} - e}{\tan[\alpha]} - s_c\right)^2 + e^2} \quad (11)$$

where  $s_c$  is the displacement of the follower,  $[\alpha]$  is the allowed pressure angle, and  $e$  is the eccentricity. Note that this paper adopts the disk cam mechanism with an aligned roller follower. Thus,  $e = 0$ , and Equation (11) can be replaced by Equation (12):

$$r_0 \geq \left| \frac{\frac{ds}{d\phi}}{\tan[\alpha]} \right| \quad (12)$$

By combining Equations (10)–(12), the contour of the designed cam can be obtained, as shown in Figure 4.

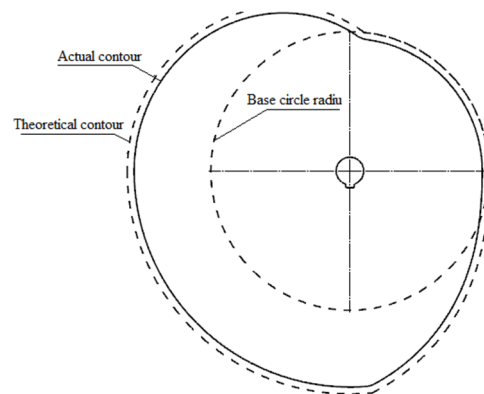


Figure 4. The contour of the designed cam.

## 3. Computational Dynamic Analysis

### 3.1. Computational Simulation of the Design Model and a Typical Model

Figure 5a displays the construction view of the design model. The commercial software MSC.ADAMS has powerful abilities in parametric modeling and can establish and solve the dynamic equations automatically. Thus, we employed ADAMS to establish the model. As shown in Figure 5a, the model consisted of two motors and a crankshaft, linkage, crosshead, piston, cylinder, cam, follower, and guide bearing. The whole parts were built with NX.UG software and imported into the ADAMS software via the Parasolid format file. After that, we finished the model in ADAMS via setting the material properties of the parts, building a kinematic pair according to the motion relationship between the parts, and creating the joint motion and the spring force. In this case, the material of the parts was set to steel,

except for the guide bearing, for which the material was set to copper. All the kinematic pairs in the model, including the revolute joints between the crankshaft and motor shaft, between the crankshaft and linkage, between the linkage and crosshead, between the cam and the other motor shaft, and the translational joints between the crosshead and its guide, between the piston and cylinder, and between the follower and the bearing, were set to ideal joints. Table 1 provides the parametric characteristics of the model. Table 2 shows the material properties of these parts.

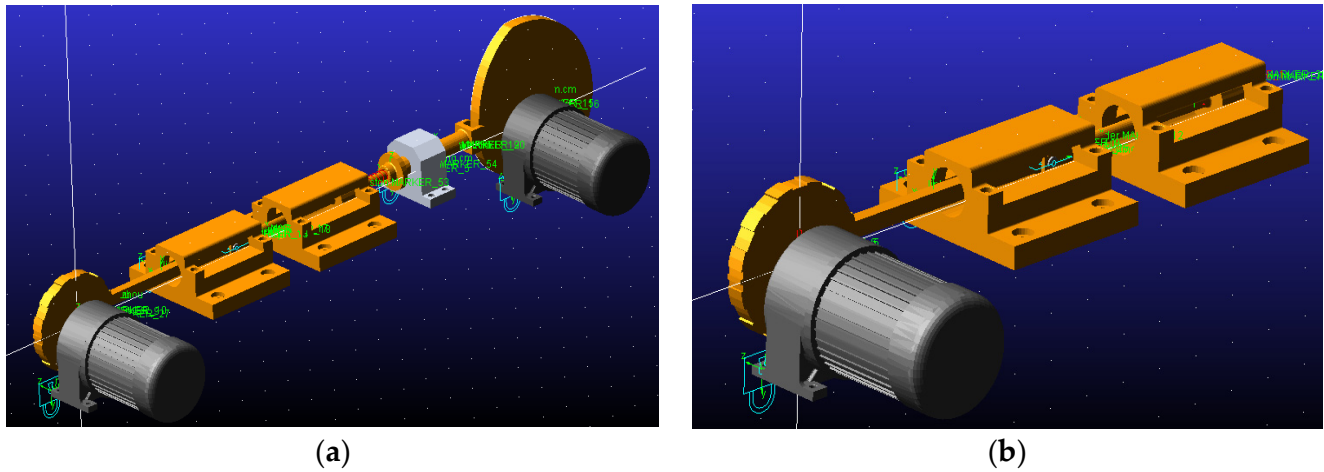


Figure 5. The model of the reciprocating compressor under ADAMS: (a) the design model and (b) the typical model.

Table 1. Simulation characteristics.

Simulation Characteristics	Value
Length of the crankshaft (mm)	120
Length of the linkage (mm)	600
Stroke of the piston (mm)	240
Radius of the piston (mm)	50
Pressure in the suction process (MPa)	0.105
Pressure in the discharge process (MPa)	0.393
Speed of the crankshaft (rpm)	500
Radius of the base circle of the cam (mm)	200
Stroke of the follower (mm)	120
Length of the spring (mm)	340
Stiffness coefficient of the spring (N/mm)	20
Damping coefficient of the spring (N/(mm*s))	0.023
Preload of the spring (N)	800
Speed of the cam (rpm)	500

Table 2. Material performance.

Material	Density (kg/mm <sup>3</sup> )	Young's Modulus (N/mm <sup>2</sup> )	Poisson's Ratio
steel	$7.801 \times 10^{-6}$	$2.07 \times 10^5$	0.29
copper	$8.906 \times 10^{-6}$	$1.19 \times 10^5$	0.326

To validate the model, a typical model of the reciprocating compressor was also established in this paper. Figure 5b displays the construction view of the typical model. The typical model had the same parametric characteristics as the design model—except for the load model, which relied on Equation (6)—and they were realized by the IF function in the ADAMS software. Equation (13) shows the IF function of the load:

$$\begin{aligned}
 &IF(MOD(time * 3000, 360) - 38.95 : 3086.6 * (20 / (740 - compressor.crosshead\_dx)) * 1.4, 824.6; \\
 &IF(MOD(time * 3000, 360) - 180 : 824.6, 824.6; \\
 &IF(MOD(time * 3000, 360) - 294.2 : 824.6 * (260 / (740 - compressor.crosshead\_dx)) * 1.4, 3086.6, 3086.6) ) )
 \end{aligned}
 \tag{13}$$

where “*compressor.crosshead\_dx*” is the measured displacement of the crosshead and piston and “*time*” is the time.

For the rigid system, ADAMS used the modified Newton–Raphson iterative algorithm to solve the dynamic differential equation and provided four integrators (including GSTIFF, WSTIFF, DSTIFF, and CONSTANT\_BDF) and three kinds of an integral formulation (including I3, SI2, and SI1). In this paper, we chose the Gear Stiff integrator (GSTIFF), which calculates fast and provides an accurate result for displacement, and integral formulation SI2, which considers the speed constraint equations and provides an accurate solution for the velocity and acceleration. During the simulation, the end time was 0.48 (s), the step time was 0.0001 (s), and the integration tolerance was  $10^{-5}$ .

### 3.2. Computational Simulation of the Design Model under a Fault State

Due to error of assembly, wear, and other factors, excessive clearance is the most common failure of the reciprocating compressor movement mechanism. The typical representatives are the clearance failures on the big end and little end of the linkage. These clearance failures are the major reasons behind abnormal vibration of the reciprocating compressor body. Therefore, this paper establishes a clearance fault model based on the design model to investigate the dynamic behavior of the moving parts under fault conditions.

The clearance faults in the joint between the crankshaft and linkage or between the linkage and crosshead can be classified as faults of the revolute joint with clearance. These faults can be simulated by setting different clearance sizes at the corresponding revolute joints (the revolute joint model can be referred to in [20]). For the contact between the journal and bearing, we applied the contact method based on the impact function available in the ADAMS function library [21]. The contact model treats the contact as a nonlinear spring damper, including a contact force model based on the Hertz contact law and a friction model based on the Coulomb friction model. The contact force is calculated by the penetration and the speed of penetration as in the following equation [22–24]:

$$F_N = \begin{cases} K\delta^n + STEP(\delta, 0, 0, d_{max}, C_{max})\dot{\delta} & \delta > 0 \\ 0 & \delta < 0 \end{cases} \quad (14)$$

where  $K$  is the stiffness coefficient that depends on the material property and the radius,  $\delta$  is the penetration,  $n$  is the deformation force exponent that equals 1.5 for the metallic contact,  $d_{max}$  is a positive real value of the boundary penetration, and  $C_{max}$  is the maximum damping coefficient, and the following is also true:

$$\begin{cases} K = \frac{4}{3\pi(h_1+h_2)} \sqrt{\frac{R_1R_2}{R_1+R_2}} \\ h_i = \frac{1-\mu_i^2}{\pi E_i} (i = 1, 2) \end{cases} \quad (15)$$

where  $R_i$  is the radius,  $\mu_i$  is the Poisson’s ratio, and  $E_i$  is the modulus of the elasticity.

The Coulomb friction force can be given by Equation (16) [22–24]:

$$F_t = -c_f F_N \frac{v_t}{|v_t|} \quad (16)$$

where  $c_f$  is the friction coefficient,  $F_N$  is the normal force, and  $v_t$  is the relative tangential velocity.

We established the fault model based on the design model in ADAMS, as Figure 5a shows. In the case of faults in the joint between the linkage and crankshaft, we set the revolute joint between the crankshaft and linkage to clearances of 0.1 mm, 0.2 mm, and 0.3 mm and set the other joints as the ideal joints. In the case of a clearance fault in the joint between the linkage and crosshead, we set the revolute joint between the linkage and crosshead to clearances of 0.1 mm, 0.2 mm, and 0.3 mm and set the other joints as the ideal joints. In the case of clearance faults in both joints of the linkage, we set the revolute joint between the linkage and crankshaft and the joint between the linkage and crosshead to

clearances of 0.1 mm, 0.2 mm, and 0.3 mm and set the other joints as the ideal joints. In processing the simulations of these cases, the contact model based on the IMPACT function was used to simulate the revolute joint with clearance. Table 3 depicts the characteristic parameters of the impact function.

**Table 3.** Characteristic parameters of impact function.

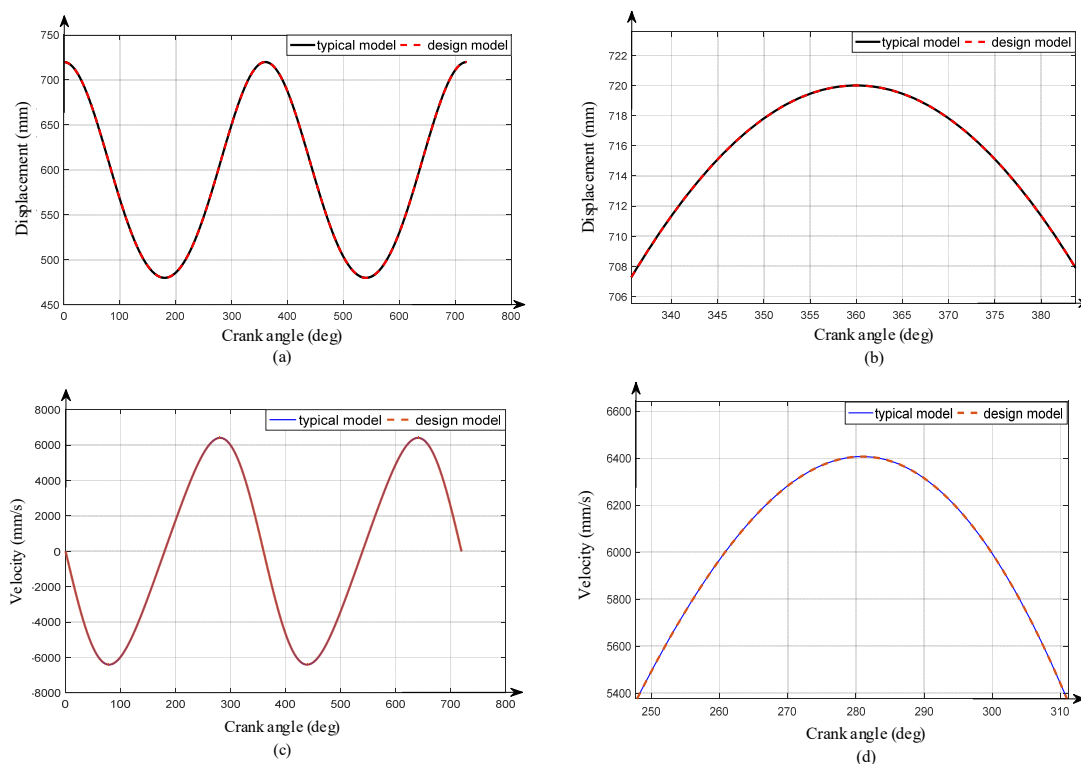
Parameter	Value
Stiffness (N/mm)	$3.36 \times 10^5$
Force exponent	1.5
Damping (N/(mm/s))	336
Penetration depth (mm)	0.1
Static coefficient	0.23
Dynamic coefficient	0.15
Stiction transition velocity (mm/s)	10
Friction transition velocity (mm/s)	100

#### 4. Results and Discuss

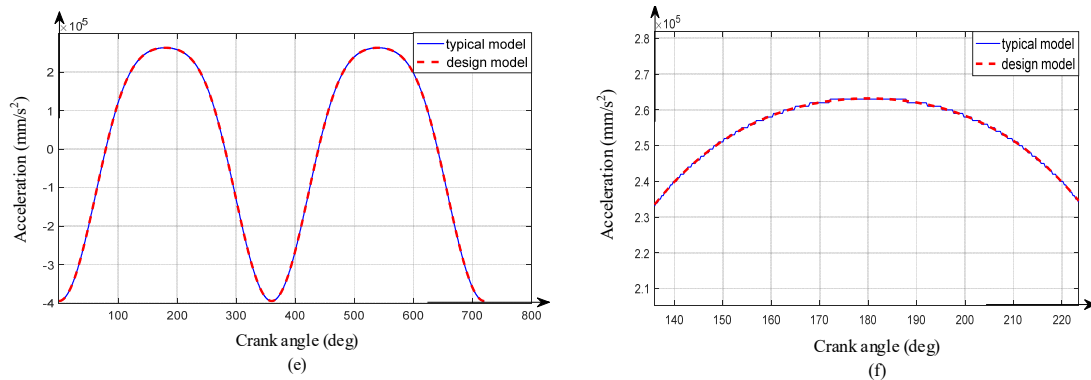
##### 4.1. Comparison between the Design Model and the Typical Model

Figure 6 displays the computational displacement, velocity, and acceleration of the translational mechanism of the design model and the typical model. Figure 6 directly shows that the dynamic responses of the design model were generally consistent with those of the typical model.

Figure 7 displays the simulated piston force of the two models. It can be seen from Figure 7 that the simulated piston forces of the two models had a similar varying trend, but there were two biases between the simulated piston force of the design model and the typical model. One was that the peak value of the force of the design model was bigger than that of the typical model. The other was that the position where the piston force varied from one process to the other process was different. These biases were caused by the characteristics of the spring that we chose. This can be greatly improved by choosing a nonlinear spring, for which the stiffness increases with an increasing deformation.



**Figure 6.** Cont.



**Figure 6.** The dynamic response of the translational mechanism in the designed model and the typical model: (a) displacement, (b) enlarged displacement, (c) velocity, (d) enlarged velocity, (e) acceleration, and (f) enlarged acceleration.

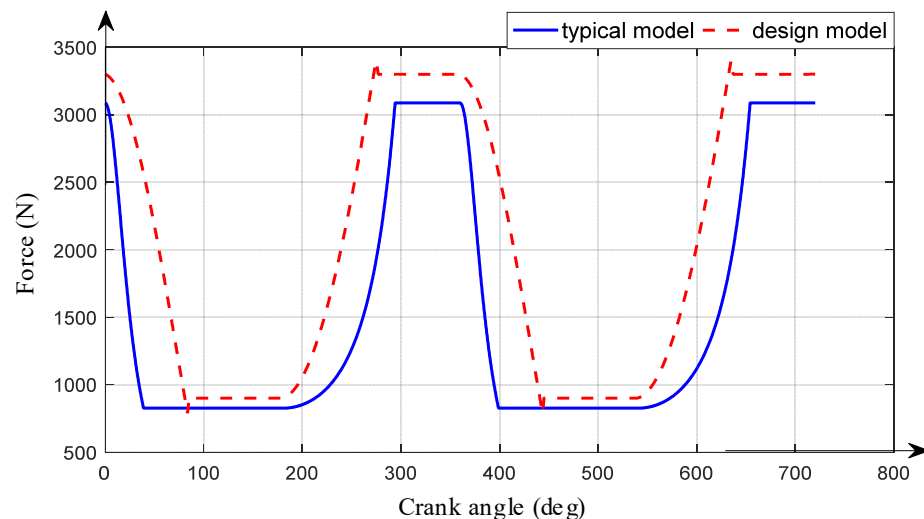
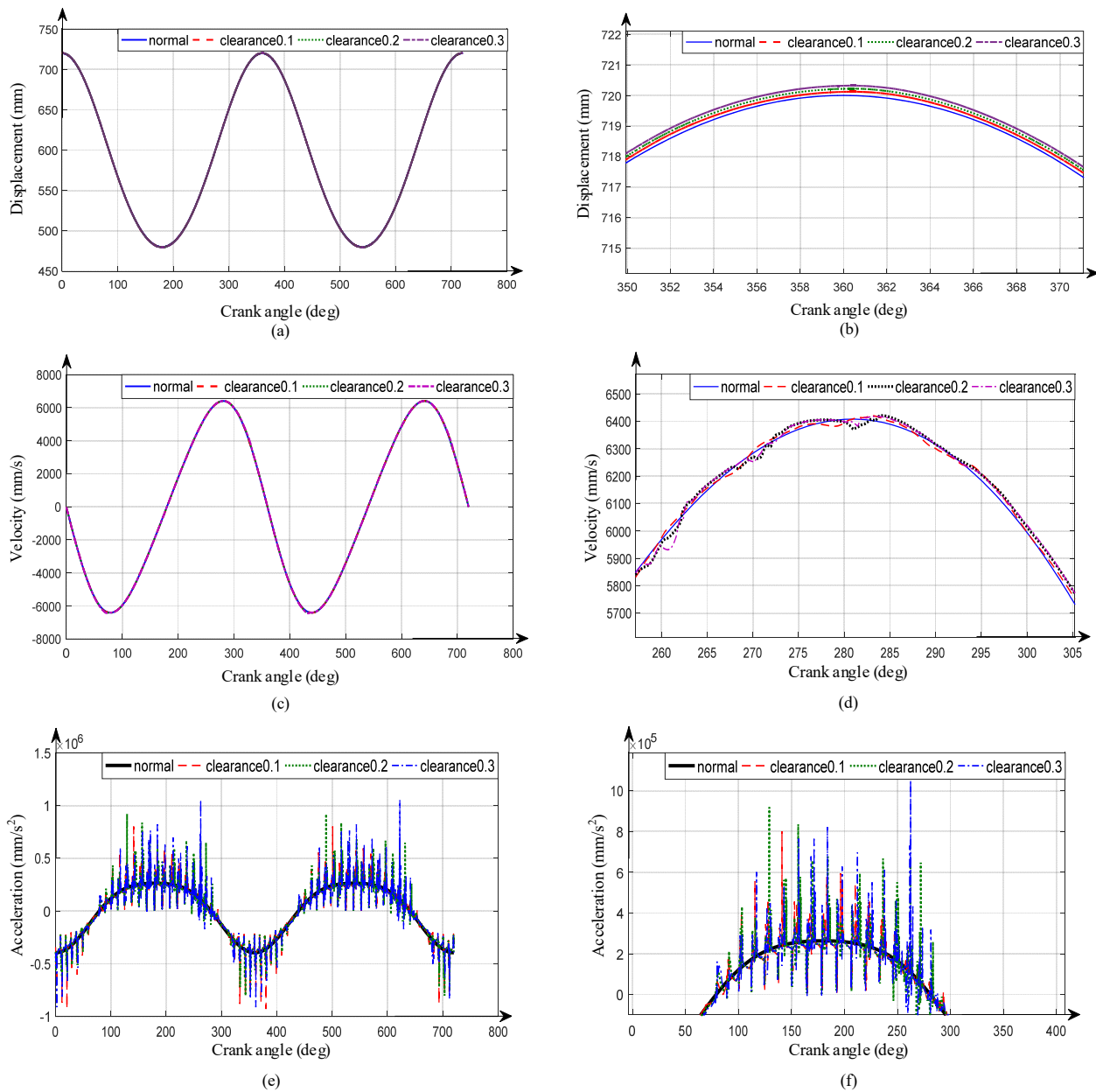


**Figure 7.** The simulated piston load of the designed model and the typical model.

Although some problems existed in the design model, it could realize the simulation of the mechanism of the reciprocating compressor. The designed model has two advantages. One is that the model, compared with the virtual model presented in the existing literature, can be processed into a physical prototype, which can enable researchers to further study the faults of the compressor. The other is that the model, compared with a real reciprocating compressor, makes it easy to investigate the translational mechanism of the compressor.

#### 4.2. Dynamic Response to the Clearance Fault of the Joint between the Linkage and the Crankshaft

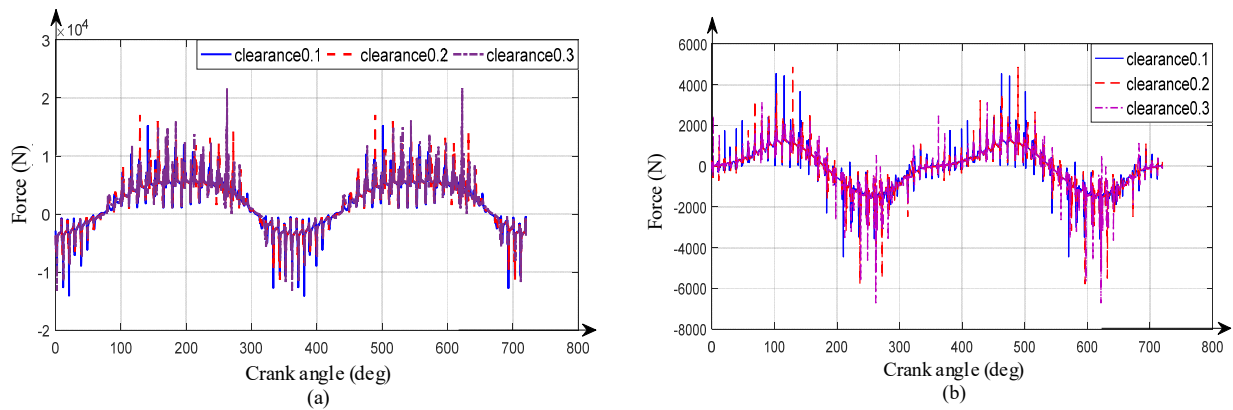
Figure 8 shows the computational displacement, velocity, and acceleration of the translational mechanism in the case of the clearance fault of the joint between the crankshaft and linkage. As shown in Figure 8, the displacement and velocity of the mechanism with clearance were consistent with those of the mechanism without clearance. Slight oscillations occurred at the curve peaks and troughs of the displacement and velocity of the mechanism with clearance. The larger clearance was, the bigger deviation values of the displacement and velocity were. The acceleration of the mechanism was greatly influenced by the clearance fault. As the clearance size increased, the curve of the acceleration oscillated more intensely and had a higher amplitude.



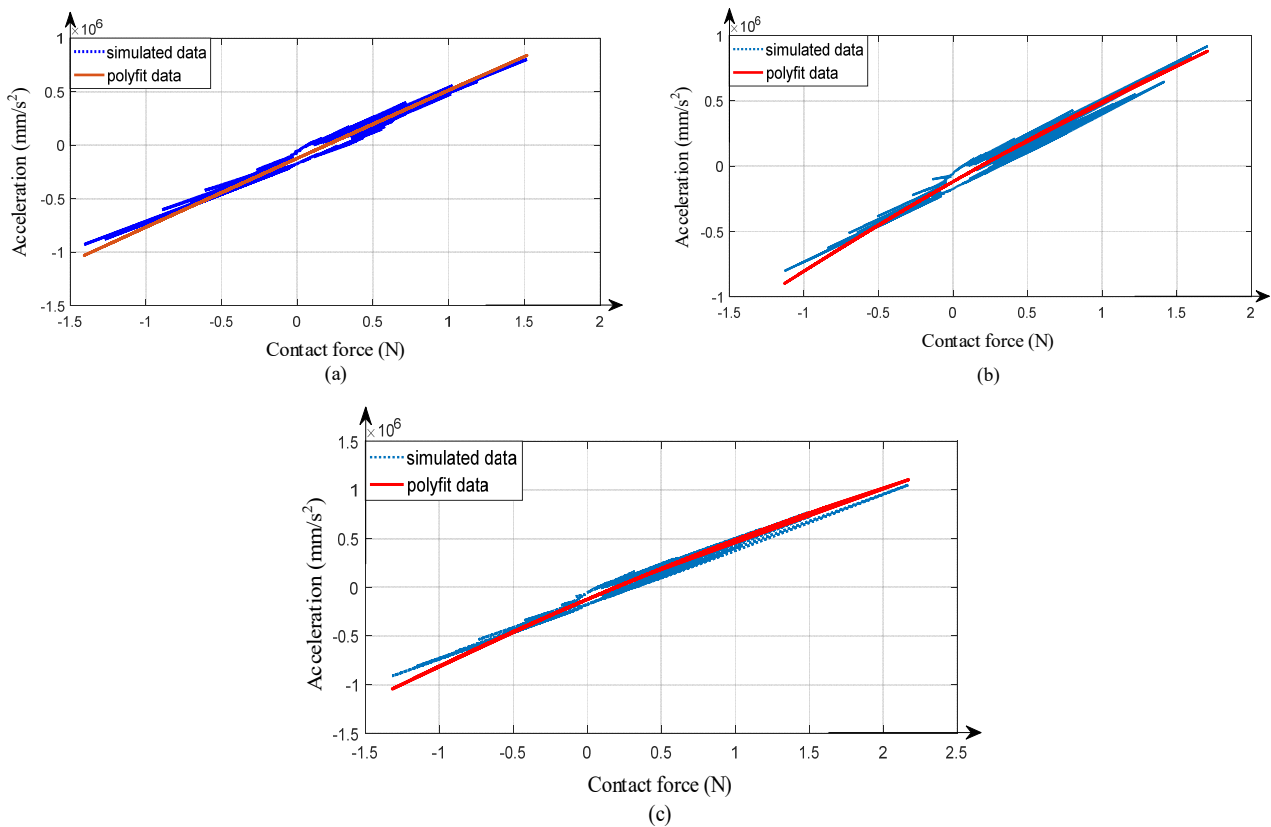
**Figure 8.** The dynamic response of the model under clearance fault in the joint between the crankshaft and linkage: (a) displacement, (b) enlarged displacement, (c) velocity, (d) enlarged velocity, (e) acceleration, and (f) enlarged acceleration.

Figure 9 shows the computational contact force between the journal and the bearing of the joint between the crankshaft and the linkage with different clearance sizes. From Figure 9, we can easily conclude that the larger the clearance was, the more violent the impacts between the journal and bearing were. In addition, the impacts mainly occurred in the horizontal direction, for which the contact force was much larger than the force in the vertical direction.

According to the two figures, we also found that the computational acceleration of the mechanism and the contact force in the horizontal direction had a similar varying trend. As shown in Figure 10, there seemed to be a proportional relationship between the acceleration of the mechanism and the contact force in the horizontal direction caused by the clearance fault. This means that the clearance fault in the joint between the crankshaft and the linkage was one of major causes of the vibration of the compressor body.



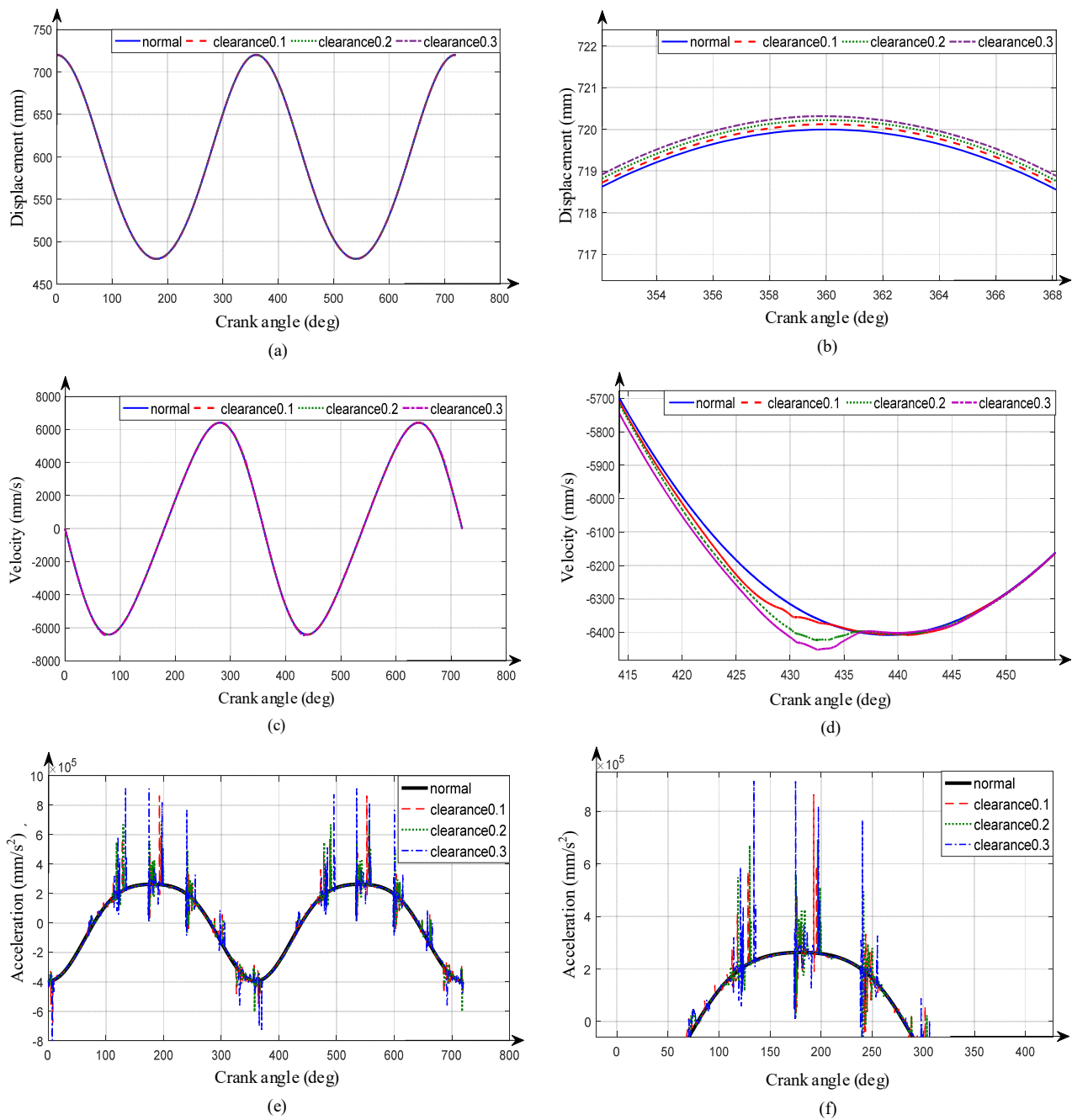
**Figure 9.** The contact force between the journal and bearing of the joint between the crankshaft and linkage: (a) horizontal direction and (b) vertical direction.



**Figure 10.** The relationship diagram of the acceleration of the mechanism and the contact force on the joint between the crankshaft and linkage: (a) clearance of 0.1 mm, (b) clearance of 0.2 mm, and (c) clearance of 0.3 mm.

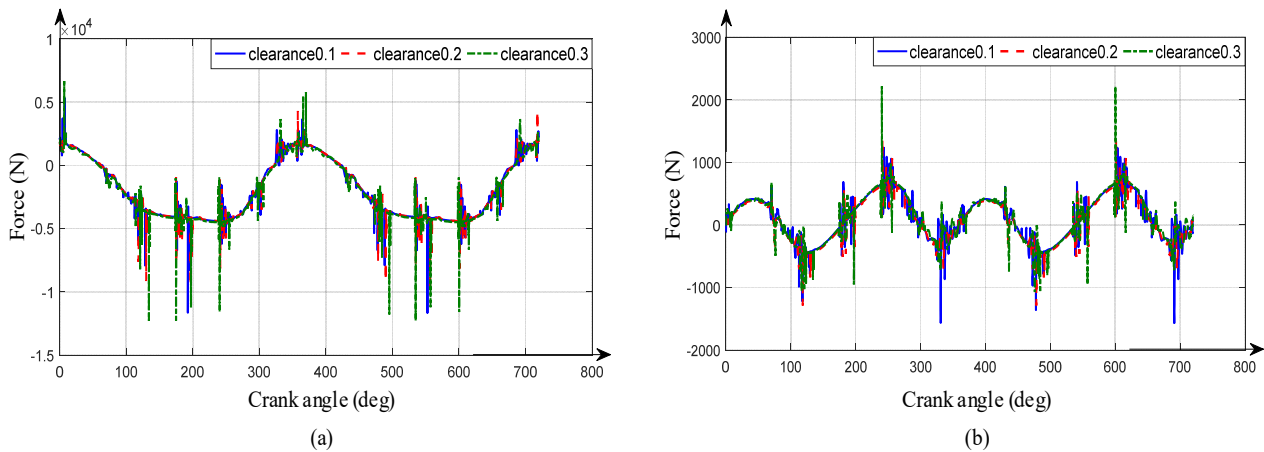
4.3. Dynamic Response to the Clearance Fault in the Joint between the Linkage and the Crosshead

Figure 11 depicts the computational displacement, velocity, and acceleration of the translational mechanism in the case of a clearance fault in the joint between the linkage and crosshead. From Figure 11, we can draw similar conclusions to those resulting from Figure 8. First, the clearance fault slightly influenced the displacement and velocity of the mechanism and greatly affected the acceleration of the mechanism. Secondly, the larger the clearance was, the more intense the curve of the acceleration oscillated, and the higher the amplitude peak that occurred.



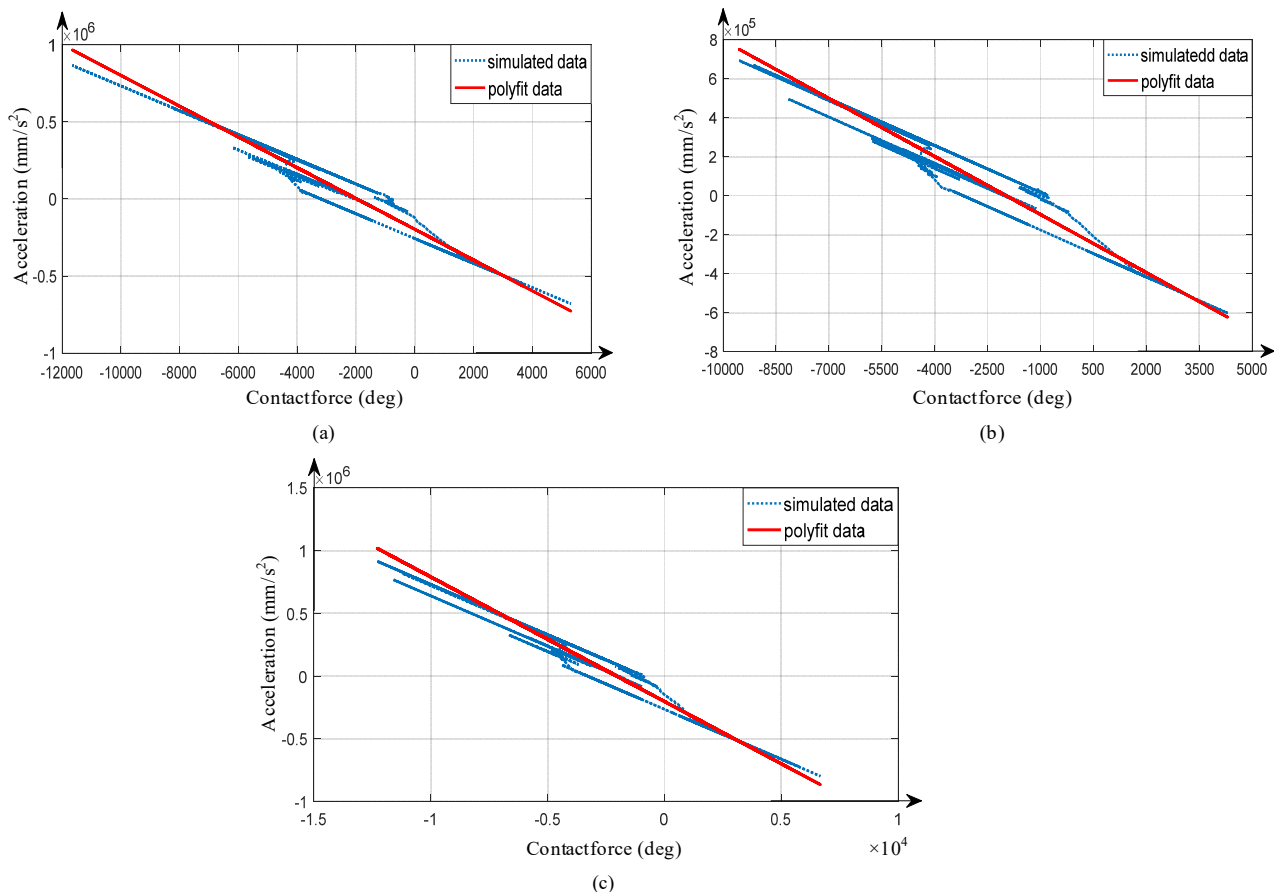
**Figure 11.** The computational dynamic response of the model with a clearance fault in the joint between the crosshead and linkage: (a) displacement, (b) enlarged displacement, (c) velocity, (d) enlarged velocity, (e) acceleration, and (f) enlarged acceleration.

Figure 12 shows the computational contact force between the journal and the bearing of the joint between the linkage and the crosshead with different clearance sizes. It can be seen from Figure 12 that the clearance greatly affected the contact force between the journal and bearing of the joint between the linkage and the crosshead. As the clearance became larger, the contact force oscillated more intensely, and more violent impacts occurred. The impacts mainly occurred in the horizontal direction, in which the contact force was much bigger than that in the vertical direction.



**Figure 12.** The contact force between the journal and bearing of the joint between the crosshead and linkage: (a) horizontal direction and (b) vertical direction.

In this case, we also found that the acceleration of the mechanism had a proportional relationship with the contact force in the horizontal direction, as shown in Figure 13. Thus, the clearance fault in the joint between the linkage and the crosshead was also one of the major causes of vibration.



**Figure 13.** The relationship diagram of the acceleration of the mechanism and the contact force on the joint between the linkage and crosshead: (a) clearance of 0.1 mm, (b) clearance of 0.2 mm, and (c) clearance of 0.3 mm.

In a word, we can get some similar conclusions in the two cases. There were several differences between the two cases, where the vibration and impact occurred intermittently in the case of a clearance fault in the joint between linkage and crosshead, but the vibration

and impact occurred almost continuously in the case of a clearance fault in the joint between the crankshaft and linkage.

4.4. Dynamic Response to the Clearance Fault in Both Joints of the Linkage

In this case, in order to study the influence of the clearance number on the vibration of the compressor body, we set both joints of the linkage to certain clearances.

Figure 14 displays the computational displacement, velocity, and acceleration of the translational mechanism in the case of a clearance fault in both joints of the linkage. As depicted in Figure 14, the displacement and velocity of the mechanism with clearance were generally consistent with those of the mechanism without clearance and were slightly affected by the clearance. The acceleration was greatly influenced by the clearance. As the clearance size increased, the acceleration oscillated more violently and displayed a higher amplitude.

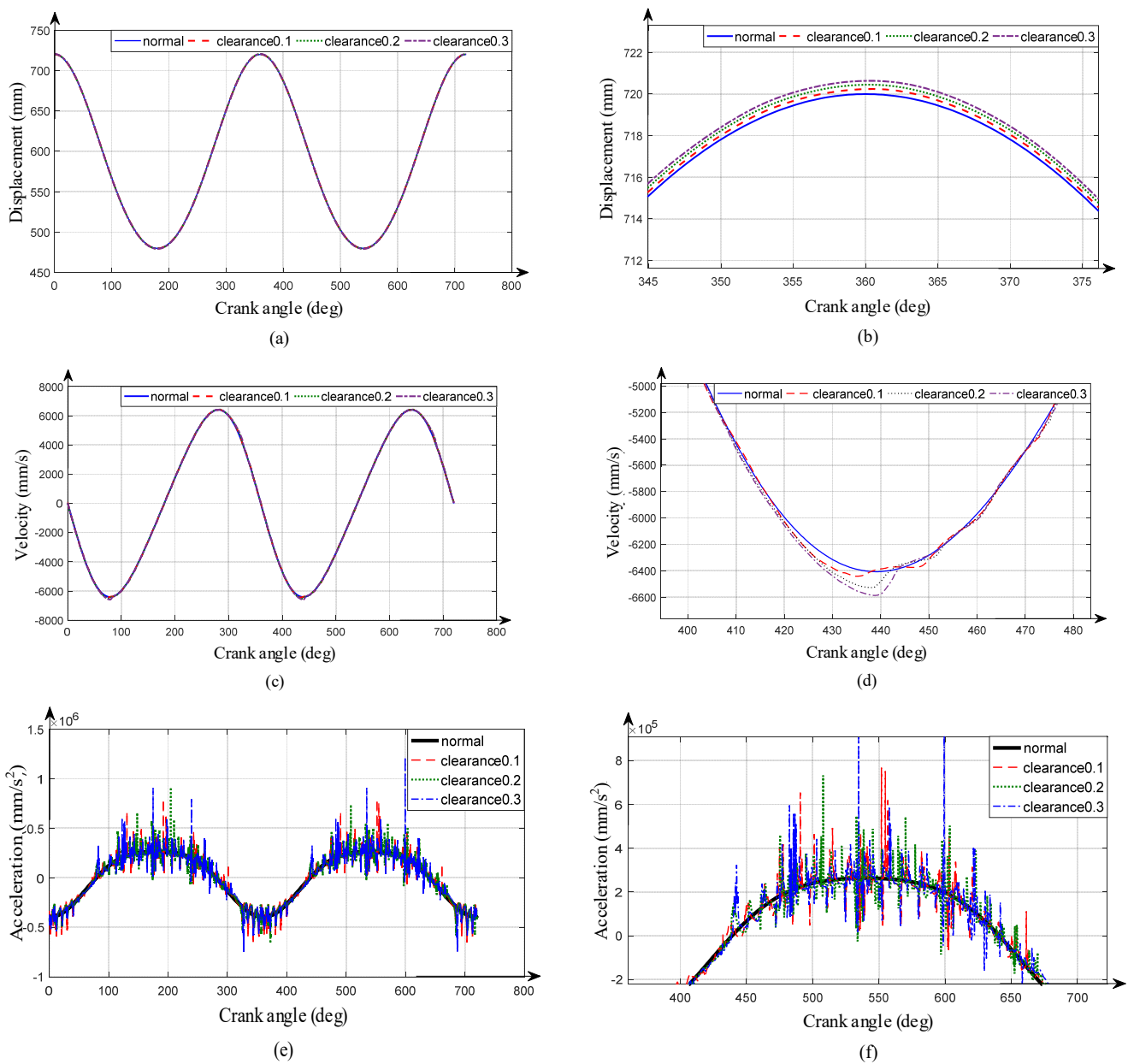
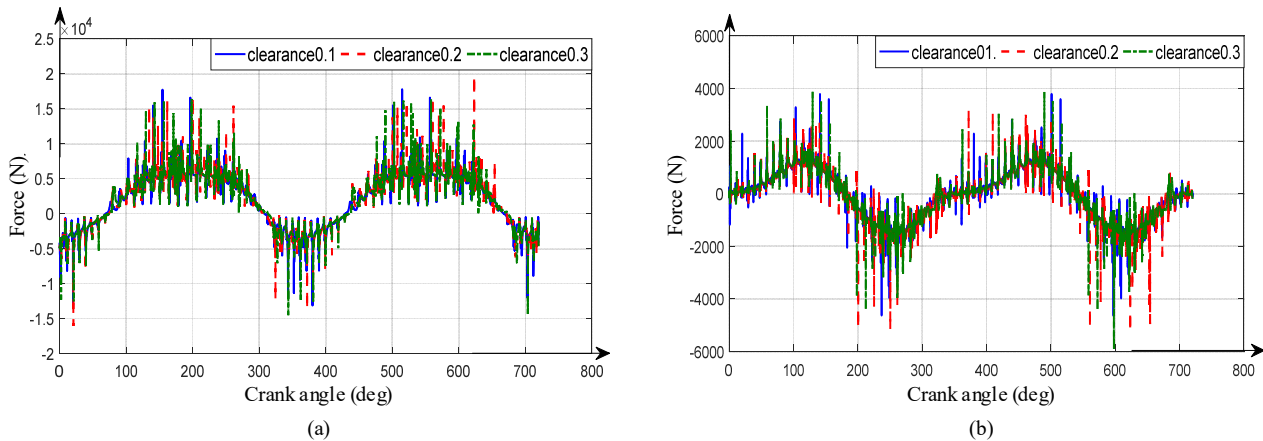
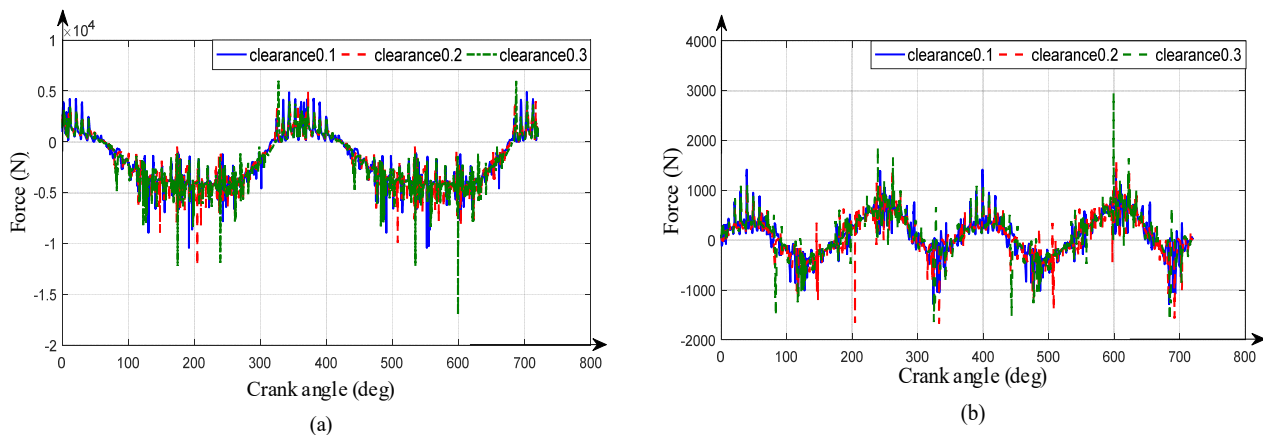


Figure 14. The computational dynamic response of the model under a clearance fault in both joints of the linkage: (a) displacement, (b) enlarged displacement, (c) velocity, (d) enlarged velocity, (e) acceleration, and (f) enlarged acceleration.

Figure 15 shows the computational contact force between the journal and the bearing of the joint between the crankshaft and linkage with different clearance sizes. Figure 16 shows the contact force between the journal and the bearing of the joint between the linkage and crosshead with different clearance sizes. From the two diagrams, we found that the contact forces on both joints of the linkage were extremely influenced by the clearance size.



**Figure 15.** The contact force of the joint between the crankshaft and linkage: (a) horizontal direction and (b) vertical direction.



**Figure 16.** The contact force of the joint between the linkage and crosshead: (a) horizontal direction and (b) vertical direction.

Compared with a single clearance fault, the vibration and impact of the reciprocating compressor system with two clearance faults became more violent, and its peak amplitude was also higher.

## 5. Conclusions

In this work, a simplified model of the moving mechanism in a reciprocating compressor was established with ADAMS software. To validate the model, we also introduced a typical model based on the ideal piston force. The simulation results show that the dynamic responses of the design model were consistent with those of the typical model. Although some biases existed, the simulated piston forces of the two models had a similar varying trend. The results demonstrate that the design model could realize the simulation of the mechanism of the reciprocating compressor. Compared with the existing model of the compressor, the design model could be processed into a physical prototype, which would enable researchers to further study the fault mechanism of the reciprocating compressor.

This work also took several typical faults in the mechanism of the reciprocating compressor into account, including the clearance fault in the joint between the crank and the connecting rod, between the connecting rod and the crosshead, and both. These faults are a major cause of the vibration of the reciprocating compressor. A simulation for the

mechanism under the above fault state, based on the design model and the IMPACT function provided in ADAMS, was carried out in this work to study the relationship between these faults and the vibration. The research results show that the size and number of clearance faults influenced the vibration of the reciprocating compressor system. As the clearance increased, the vibration was more violent, and the amplitude of the vibration was much higher. Furthermore, the clearance number greatly affected the vibration, and the greater the clearance value, the greater the vibration.

**Author Contributions:** S.X., Q.X. and M.S. contributed equally to this work and should be considered co-first authors. In this paper, Z.Z. mainly assisted the first author to debug the simulation program and modify the grammar of this paper. All authors have read and agreed to the published version of the manuscript.

**Funding:** This research was funded by the Natural Science Foundation of Fujian province (Grant No. 2020J01432), the major training project of Ningde Normal University (Grant No. 2020ZDK01), and the Innovation Team of Ningde Normal University (No. 2020T02).

**Conflicts of Interest:** The authors declare no conflict of interest.

## References

1. Ali, S.M.; Hui, K.; Hee, L.; Leong, M.S. Automated valve fault detection based on acoustic emission parameters and support vector machine. *Alex. Eng. J.* **2018**, *57*, 491–498. [[CrossRef](#)]
2. Qi, G.; Zhu, Z.; Erqinhu, K.; Chen, Y.; Chai, Y.; Sun, J. Fault-diagnosis for reciprocating compressors using big data and machine learning. *Simul. Model. Pract. Theory* **2018**, *80*, 104–127. [[CrossRef](#)]
3. Qin, Q.; Jiang, Z.-N.; Feng, K.; He, W. A novel scheme for fault detection of reciprocating compressor valves based on basis pursuit, wave matching and support vector machine. *Measurement* **2012**, *45*, 897–908. [[CrossRef](#)]
4. Zhang, Y.; Ji, J.; Ma, B. Fault diagnosis of reciprocating compressor using a novel ensemble empirical mode decomposition-convolutional deep belief network. *Measurement* **2020**, *156*, 107619. [[CrossRef](#)]
5. Farzaneh-Gord, M.; Khoshnazar, H. Valve fault detection for single-stage reciprocating compressors. *J. Nat. Gas Sci. Eng.* **2016**, *35*, 1239–1248. [[CrossRef](#)]
6. Guo, F.Y.; Zhang, Y.C.; Wang, Y.; Wang, P.; Ren, P.J.; Guo, R.; Wang, X.Y. Fault Detection of Reciprocating Compressor Valve Based on One-Dimensional Convolutional Neural Network. *Math. Probl. Eng.* **2020**, *2020*, 8058723. [[CrossRef](#)]
7. Pichler, K.; Lughofer, E.; Pichler, M.; Buchegger, T.; Klement, E.P.; Huschenbett, M. Fault detection in reciprocating compressor valves under varying load conditions. *Mech. Syst. Signal Process.* **2016**, *70–71*, 104–119. [[CrossRef](#)]
8. Cerrada, M.; Macancela, J.C.; Cabrera, D.; Estupiñan, E.; Sánchez, R.V.; Medina, R. Reciprocating Compressor Multi-Fault Classification Using Symbolic Dynamics and Complex Correlation Measure. *Appl. Sci.* **2020**, *10*, 2512. [[CrossRef](#)]
9. Potočník, P.; Govekar, E. Semi-supervised vibration-based classification and condition monitoring of compressors. *Mech. Syst. Signal Process.* **2017**, *93*, 51–65. [[CrossRef](#)]
10. Chen, J.; Randall, R.; Peeters, B. Advanced diagnostic system for piston slap faults in IC engines, based on the non-stationary characteristics of the vibration signals. *Mech. Syst. Signal Process.* **2016**, *75*, 434–454. [[CrossRef](#)]
11. Geng, Z.; Chen, J. Investigation into piston-slap-induced vibration for engine condition simulation and monitoring. *J. Sound Vib.* **2005**, *282*, 735–751. [[CrossRef](#)]
12. Ndiaye, D.; Bernier, M. Dynamic model of a hermetic reciprocating compressor in on-off cycling operation (Abbreviation: Compressor dynamic model). *Appl. Therm. Eng.* **2010**, *30*, 792–799. [[CrossRef](#)]
13. Yang, B.; Bradshaw, C.R.; Groll, E.A. Modeling of a semi-hermetic CO<sub>2</sub> reciprocating compressor including lubrication submodels for piston rings and bearings. *Int. J. Refrig.* **2013**, *36*, 1925–1937. [[CrossRef](#)]
14. Farzaneh-Gord, M.; Niazmand, A.; Deymi-Dashtebayaz, M.; Rahbari, H.R. Thermodynamic analysis of natural gas reciprocating compressors based on real and ideal gas models. *Int. J. Refrig.* **2015**, *56*, 186–197. [[CrossRef](#)]
15. Link, R.; Deschamps, C.J. Numerical modeling of startup and shutdown transients in reciprocating compressors. *Int. J. Refrig.* **2011**, *34*, 1398–1414. [[CrossRef](#)]
16. Pont, A.; López, J.; Rigola, J.; Pérez-Segarra, C. Numerical dynamic analysis of reciprocating compressor mechanism. Parametric studies for optimization purposes. *Tribol. Int.* **2017**, *105*, 1–14. [[CrossRef](#)]
17. Almasi, A. A new study and model for the mechanism of process reciprocating compressors and pumps. *Proc. Inst. Mech. Eng. Part E-J. Process. Mech. Engineering* **2010**, *224*, 143–147. [[CrossRef](#)]
18. Zhao, H.; Xu, M.; Wang, J.; Li, Y. A parameters optimization method for planar joint clearance model and its application for dynamics simulation of reciprocating compressor. *J. Sound Vib.* **2015**, *344*, 416–433.
19. Xiao, Q. *Research on Simulation Device and Fault Simulation of Reciprocating Compressor Transmission Mechanism*; University Press: Shanghai, China, 2019.

20. Li, Y.; Wang, C.; Huang, W. Dynamics analysis of planar rigid-flexible coupling deployable solar array system with multiple revolute clearance joints. *Mech. Syst. Signal Process.* **2018**, *117*, 188–209. [[CrossRef](#)]
21. Xiao, S.; Liu, S.; Jiang, F.; Song, M.; Cheng, S. Nonlinear dynamic response of reciprocating compressor system with rub-impact fault caused by subsidence. *J. Vib. Control.* **2019**, *25*, 1737–1751. [[CrossRef](#)]
22. Tian, Q.; Flores, P.; Lankarani, H.M. A comprehensive survey of the analytical, numerical and experimental methodologies for dynamics of multibody mechanical systems with clearance or imperfect joints. *Mech. Mach. Theory* **2018**, *122*, 1–57. [[CrossRef](#)]
23. Xiao, S.; Liu, S.; Song, M.; Ang, N.; Zhang, H. Coupling rub-impact dynamics of double translational joints with subsidence for time-varying load in a planar mechanical system. *Multibody Syst. Dyn.* **2019**, *48*, 451–486. [[CrossRef](#)]
24. Xiao, S.; Liu, S.; Wang, H.; Lin, Y.; Song, M.; Zhang, H. Nonlinear dynamics of coupling rub-impact of double translational joints with subsidence considering the flexibility of piston rod. *Nonlinear Dyn.* **2020**, *100*, 1203–1229. [[CrossRef](#)]